IOP Publishing Nanotechnology
Nanotechnology 32 (2021) 135401 (11pp) https://doi.org/10.1088/1361-6528/abd20c

The exceptionally high thermal conductivity after 'alloying' two-dimensional gallium nitride (GaN) and aluminum nitride (AlN)

Huimin Wang[1,2,3,7], Donghai Wei[3,4,7], Junfei Duan[4], Zhenzhen Qin[5], Guangzhao Qin[3,*], Yagang Yao[1,6,*] and Ming Hu[2,*]

[1] National Laboratory of Solid State Microstructures, College of Engineering and Applied Sciences, Jiangsu Key Laboratory of Artificial Functional Materials, and Collaborative Innovation Center of Advanced Microstructures, Nanjing University, Nanjing 210093, People's Republic of China
[2] Department of Mechanical Engineering, University of South Carolina, Columbia, SC 29208, United States of America
[3] State Key Laboratory of Advanced Design and Manufacturing for Vehicle Body, College of Mechanical and Vehicle Engineering, Hunan University, Changsha 410082, People's Republic of China
[4] School of Materials Science and Engineering, Changsha University of Science and Technology, Changsha 410004, People's Republic of China
[5] School of Physics and Microelectronics, Zhengzhou University, Zhengzhou 450001, People's Republic of China
[6] Division of Nanomaterials, Suzhou Institute of Nano-Tech and Nano-Bionics, Nanchang, Chinese Academy of Sciences, Nanchang 330200, People's Republic of China

E-mail: gzqin@hnu.edu.cn, ygyao2018@nju.edu.cn and hu@sc.edu

Received 3 October 2020, revised 29 November 2020
Accepted for publication 8 December 2020
Published 6 January 2021

Abstract

Alloying is a widely employed approach for tuning properties of materials, especially for thermal conductivity which plays a key role in the working liability of electronic devices and the energy conversion efficiency of thermoelectric devices. Commonly, the thermal conductivity of an alloy is acknowledged to be the smallest compared to the parent materials. However, the findings in this study bring some different points of view on the modulation of thermal transport by alloying. The thermal transport properties of monolayer GaN, AlN, and their alloys of $Ga_xAl_{1-x}N$ are comparatively investigated by solving the Boltzmann transport equation (BTE) based on first-principles calculations. The thermal conductivity of $Ga_{0.25}Al_{0.75}N$ alloy (29.57 Wm^{-1} K^{-1}) and $Ga_{0.5}Al_{0.5}N$ alloy (21.49 Wm^{-1} K^{-1}) are found exceptionally high to be between AlN (74.42 Wm^{-1} K^{-1}) and GaN (14.92 Wm^{-1} K^{-1}), which violates the traditional knowledge that alloying usually lowers thermal conductivity. The mechanism resides in that, the existence of Al atoms reduces the difference in atomic radius and masses of the $Ga_{0.25}Al_{0.75}N$ alloy, which also induces an isolated optical phonon branch around 18 THz. As a result, the scattering phase space of $Ga_{0.25}Al_{0.75}N$ is largely suppressed compared to GaN. The microscopic analysis from the orbital projected electronic density of states and the electron localization function further provides insight that the alloying process weakens the polarization of bonding in $Ga_{0.25}Al_{0.75}N$ alloy and leads to the increased thermal conductivity. The exceptionally high thermal conductivity of the $Ga_xAl_{1-x}N$ alloys and the underlying mechanism as revealed in this study would bring valuable insight for the future research of materials with applications in high-performance thermal management.

Supplementary material for this article is available online

Keywords: thermal transport, alloy, isolated optical phonon

[7] These authors have contributed equally to the work.
[*] Authors to whom any correspondence should be addressed.

branch, electronic bonding, first-principles

(Some figures may appear in colour only in the online journal)

Introduction

Two-dimensional (2D) materials, especially the semiconductors, are attracting lots of attentions due to their outstanding physical, chemical, and mechanical properties, which promise wide applications in transistors [1, 2], light-emitting diodes [3], optoelectronic devices [4], energy related fields [5], etc. The classes of 2D materials include group-IV monolayers (graphene [6, 7], germanene [8, 9], silicene [10, 11], etc), transition metal dichalcogenides (MoS_2 [12, 13], $MoSe_2$ [14], etc), group-III nitrides monolayers (BN [15], AlN [16, 17] and GaN [18, 19] etc), All these 2D materials have been extensively investigated both in theoretical calculations and experiments. With the successful applications of gallium nitride (GaN) in the field of blue light-emitting diodes [19], ultraviolet optoelectronics [20, 21], etc, the monolayer GaN attracts considerable interest due to the expected unique adjustable electronic and magnetic properties [22, 23]. Moreover, monolayer aluminum nitride (AlN) is also a wide direct bandgap semiconductor [24] sharing a similar honeycomb structure as monolayer GaN, which shows promising wide applications in lots of fields.

Thermal conductivity, a fundamental property of materials, has always been the focus of attention because of its vital role in determining the working liability of electronic devices or the energy conversion efficiency of thermoelectric devices [25]. Currently, with the increasing requirements for improving the performance of micro-/nanodevices, it is really difficult to achieve the physical and chemical properties for these requirements with a single crystal as the fundamental materials. Various methods, such as nano crystallization [26, 27], heterojunction [16, 28], etc, have been implemented to improve the performance of materials. Among these methods, alloying is an excellent method with wide applications for tuning the property of materials, such as bulk materials [29], superlattices [24, 30], 2D structures [31, 32], etc, to optimize and widen their potential applications. Lots of studies have been conducted to explore the possible modulation of thermal transport by alloying two different materials. For instance, Gu *et al* demonstrates that the lattice thermal conductivity of single-layer $MoS_{2(1-x)}Se_{2x}$ alloy is lower than its corresponding pure crystals of MoS_2 and $MoSe_2$, and when $x = 25\%$, the thermal conductivity of the alloy reaches the minimum, being only 10% of MoS_2 [33]. Moreover, Ma *et al* illuminated that only a small amount of alloying (where x is tiny) to form $Al_xGa_{1-x}N$, $In_xGa_{1-x}N$, and $In_xAl_{1-x}N$ alloys could significantly reduce the thermal conductivity of the pristine materials [34].

In all these studies, the thermal conductivity of the alloy is found to be smaller than both the two pristine component materials, especially for the 25% alloy, which has been becoming a common knowledge in literature. However, the findings in this study brings some different point of view on the modulation of thermal transport by alloying.

In this paper, the thermal transport properties of monolayer $Ga_xAl_{1-x}N$, being the alloy of monolayer GaN and AlN, and the corresponding pure crystals are comparably investigated. The thermal conductivity of $Ga_{0.25}Al_{0.75}N$ is found exceptionally high as the alloy of GaN and AlN, which breaks the traditional knowledge that alloying usually leads to a lower thermal conductivity. Detailed analysis shows that the reduced atomic radius and masses difference in the $Ga_{0.25}Al_{0.75}N$ alloy have a positive effect on the symmetry-based selection rule of phonon–phonon scattering compared to the GaN. Additionally, the isolated optical phonon branch around 18 THz emerged in $Ga_{0.25}Al_{0.75}N$ could be responsible for its exceptionally high thermal conductivity. Moreover, the mode level analysis of phonon group velocity, scattering rate, Grüneisen parameter, and volume in phase space, and further fundamental analysis based on the electronic structures are performed to provide deep insight into the unusual phenomenon. The exceptionally high thermal conductivity of $Ga_{0.25}Al_{0.75}N$ achieved in this study by alloying could have great inspiration for the research of more alloying materials in future aiming at high-performance thermal management.

Methods

All the first-principles calculations are performed based on density functional theory, using the Vienna *ab initio* simulation package (VASP) [35] along with the Perdew–Burke–Ernzerhof (PBE) implementation of the generalized gradient approximation (GGA) [36] for the exchange-correlation functional. The kinetic energy cutoff of wave function is set as 2.5 times the maximal recommended cutoff in the pseudopotentials for high precision calculations [37]. The 2D monolayer system is placed in the *xy*-plane with a large vacuum spacing (∼20 Å) along the *out-of-plane* direction, which is used to avoid the interactions between layers due to the periodic boundary conditions. All the atoms are allowed to relax with the maximal Hellmann–Feynman force convergence threshold being 1×10^{-7} eV $Å^{-1}$. All geometries are fully optimized with $15 \times 15 \times 1$ Monkhorst–Pack [38] *k*-points used for sampling the first Brillouin zone of AlN, GaN, and $Ga_xAl_{1-x}N$ (the alloy of AlN and GaN).

In previous studies, the virtual crystal approximation (VCA) or the equilibrium molecular dynamics based Green–Kubo (EMD-GK) methods were employed to study the thermal conductivity of the pure crystal and alloys [39–42]. However, the lifetimes of high-frequency phonons in alloys cannot be accurately predicted by the VCA approach. Meanwhile, the limited calculation accuracy as well as the finitely available potentials in the molecular dynamics simulations make it difficult to apply the EMD-GK method to novel systems. Thus, we directly constructed the unit cell of

$Ga_xAl_{1-x}N$ alloys and calculated their thermal conductivity from the *state-of-art* first-principles

For the studies of the $Ga_xAl_{1-x}N$ alloys, the proportions of 25%, 50%, and 75% contents are considered with a $2 \times 2 \times 1$ supercell, where $x = 0.25$, 0.5, and 0.75, respectively. Due to the equivalent positions with the $P\bar{6}M2$ symmetry, there is only one possible configuration for the 25%, 50%, and 75% alloys, respectively. As for the simulations of alloys with other proportions, larger unit cells are necessary. Because of the huge computing resources demanding with the large unit cells, herein we only study the three proportions (25%, 50%, and 75%) of the $Ga_xAl_{1-x}N$ alloys. In such calculations, the alloy is treated as a mixed crystal of two different materials, which is different from the amorphous case.

The harmonic and anharmonic interatomic force constants (IFCs) are calculated by the finite displacement difference method. Based on the optimized structure, $5 \times 5 \times 1$ supercells containing 50 atoms are constructed to calculate the phonon dispersion of the parent materials of AlN and GaN, and a $3 \times 3 \times 1$ supercell containing 72 atoms is constructed to calculate the phonon dispersion of $Ga_xAl_{1-x}N$ alloys. In addition, for the direct comparison of phonon dispersions of AlN and GaN with $Ga_xAl_{1-x}N$ alloys, the unit cell, structural optimization, and phonon dispersions of AlN and GaN are also calculated following the similar procedure of $Ga_xAl_{1-x}N$ alloys. After diagonalizing the harmonic dynamical matrix, the phonon dispersions can be obtained by employing the Phonopy package [43].

The cutoff radius is used in anharmonic IFCs' calculations to discard atomic interactions when the distance is larger than the range of physical relevant anharmonic interactions. Born effective charges and dielectric permittivity tensor are considered to correct the description of long-range electrostatic interactions. With the harmonic and anharmonic IFCs, the thermal conductivity is calculated by solving phonon BTE as implemented in the ShengBTE package [44]. The phonon relaxation time (τ) is inversely proportional to the phonon scattering rate, which includes both absorption and emission processes involving three phonons. The thickness of monolayer AlN, GaN and $Ga_xAl_{1-x}N$ alloys are chosen as the *van der Walls* diameters of 3.1, 3.74, and 3.74 Å, respectively, which are used for the calculations of effective thermal conductivity and other related parameters. Note that the thermal conductivity is along the in-plane directions, which is isotropic for AlN, GaN, and their $Ga_xAl_{1-x}N$ alloys.

Results and discussions

Like graphene, all the monolayer AlN, GaN, and their alloy of $Ga_xAl_{1-x}N$ possess planar hexagonal honeycomb structural configurations, belonging to the same $P\bar{6}M2$ space group. The optimized lattice parameters of the three systems are 3.126, 3.255, and 6.318 Å with 2, 2, and 8 atoms in the unit cell, respectively. As shown in figure 1, the $Ga_xAl_{1-x}N$ ($x = 0.25$, 0.5, 0.75) is an alloy formed by uniformly mixing AlN and GaN (inset sketch in figure 1). The $Ga_{0.25}Al_{0.75}N$ alloy

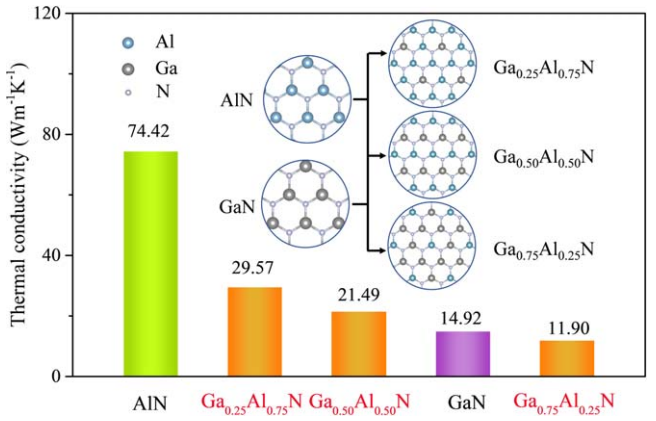

Figure 1. The comparison of the lattice thermal conductivity of AlN, GaN, and their alloys of $Ga_{0.25}Al_{0.75}N$, $Ga_{0.50}Al_{0.50}N$ and $Ga_{0.75}Al_{0.25}N$ at 300 K. Inset: the formation process of the alloy $Ga_xAl_{1-x}N$, which is a uniform mixture of AlN and GaN.

exhibits the highest thermal conductivity (29.57 Wm^{-1} K^{-1}) in the three alloy configurations compared to $Ga_{0.5}Al_{0.5}N$ (21.49 Wm^{-1} K^{-1}) and $Ga_{0.75}Al_{0.25}N$ (11.90 Wm^{-1} K^{-1}). In the following, we will mainly focus on the representative $Ga_{0.25}Al_{0.75}N$ alloy for further analysis and discussion.

Note that, the thermal conductivity of the monolayer AlN reported by Zhao *et al* was ~264.1 Wm^{-1} K^{-1}, which is calculated by conducting the classical non-equilibrium molecular dynamics simulations through the Müller–Plathe (MP) algorithm as implemented in LAMMPS [45]. The result is larger than that calculated in this work by employing the method of solving the *state-of-art* first principles based Boltzmann transport equation (BTE), which uses the GGA-PBE pseudopotentials to make the results precise and not depending on artificial parameters. It is widely known that the classical MD method suffers from the accuracy of the empirical potential, which may be the main reason for the discrepancy between the results.

Figure 2(a) shows that the thermal conductivity of $Ga_{0.25}Al_{0.75}N$ decreases with the increasing temperature, showing a normal $\kappa \sim 1/T$ dependence which is different from GaN [37]. The reason might lie in the existence of Al atoms in $Ga_{0.25}Al_{0.75}N$ compared to the GaN. Comparing the two different methods of iteration and RTA, it is clearly shown that difference of thermal conductivity between iteration and RTA for the monolayer $Ga_{0.25}Al_{0.75}N$ is not as large as monolayer AlN but much larger than GaN. Such phenomenon means that there are more normal processes in monolayer $Ga_{0.25}Al_{0.75}N$ than GaN but less than AlN. The difference between the two methods lies in that the RTA method cannot distinguish the resistive Umklapp process and the non-resistive Normal process as well as failing to take the effect of phonon hydrodynamics into account [46, 47].

It is worth noting that the thermal conductivity of monolayer $Ga_{0.25}Al_{0.75}N$ and $Ga_{0.50}Al_{0.50}N$ at room temperature lies in the middle of the thermal conductivities of the corresponding pristine components of monolayer AlN (74.42 Wm^{-1} K^{-1}) and monolayer GaN (14.92 Wm^{-1} K^{-1}) (figure 1). Such phenomenon of unusual high thermal

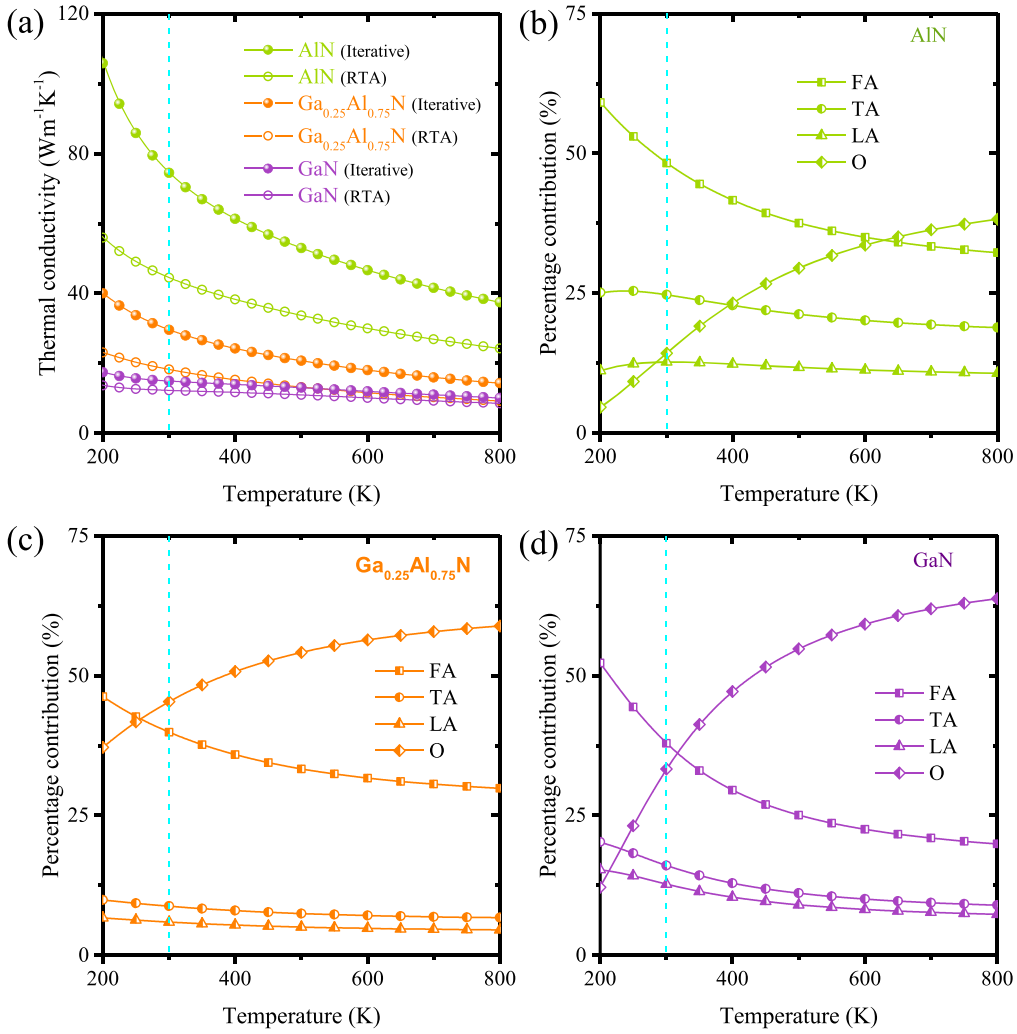

Figure 2. (a) Temperature dependent lattice thermal conductivity of monolayer AlN, $Ga_{0.25}Al_{0.75}N$, and GaN, where both the results from RTA and iterative methods are presented. (b)–(d) Temperature dependent percentage contribution to κ_L of out-of-plane flexural acoustic (FA) phonon branch, in-plane transverse acoustic (TA) phonon branch, in-plane longitudinal acoustic (LA) phonon branch and the optical (O) phonon branches for (b) AlN, (c) $Ga_{0.25}Al_{0.75}N$ and (d) GaN, respectively.

conductivity of the monolayer $Ga_xAl_{1-x}N$ systems is highly unexpected because the thermal conductivity of the alloy should be smaller than both the two pristine materials as revealed in previous studies. For instance, the thermal conductivity of the alloy of Mg_2Si and Mg_2Sn (being $Mg_2Si_xSn_{1-x}$) is smaller than both Mg_2Si and Mg_2Sn [32]. Meanwhile, the thermal conductivity of the bulk wurtzite AlN, GaN, and their 50% alloy of $Ga_{0.5}Al_{0.5}N$ is also surveyed which gives the value of 303.28, 280.09, and 151.08 Wm^{-1} K^{-1}, respectively. It is found that the thermal conductivity of the $Ga_{0.5}Al_{0.5}N$ alloy in bulk form is lower than both the parent materials, which agrees very well with the common knowledge (see supplemental materials (available online at stacks.iop.org/NANO/32/135401/mmedia) for more detailed analysis). Thus, the unusually large thermal conductivity of the 2D form $Ga_xAl_{1-x}N$ alloy ($x = 0.25$, 0.50) is exceptional as the alloy of GaN and AlN, which breaks the general rule that the alloy holds the lowest thermal conductivity compared to the pure component materials.

Note that, the disorder including mass and force field commonly lead to the reduced thermal conductivity in alloys by enhancing the scattering of phonons. In this study, the mass disorder is included by directly specifying the atomic masses of Ga and Al atoms during all the calculations, respectively. Moreover, by using the pseudopotential and exchange-correlation functionals of Ga and Al atoms, respectively, in the alloy, the force field disorder are also effectively included in our calculations. With the effect of disorders fully included, the thermal conductivity of $Ga_{0.25}Al_{0.75}N$ still stands out visibly. It is well known that phonons are the dominant carriers for heat transfer when the carrier concentration of electrons is not higher than 1×10^{20} cm^{-3} as revealed in previous study [48]. Here, in the monolayer $Ga_{0.25}Al_{0.75}N$ alloys, the built-in polarization electric fields cannot be found distinctly, and the electron-phonon interaction would not have a significant effect on the thermal transport. The effect of electron–phonon interaction on the thermal conductivity can be investigated in future studies, especially when carrier concentration is relatively

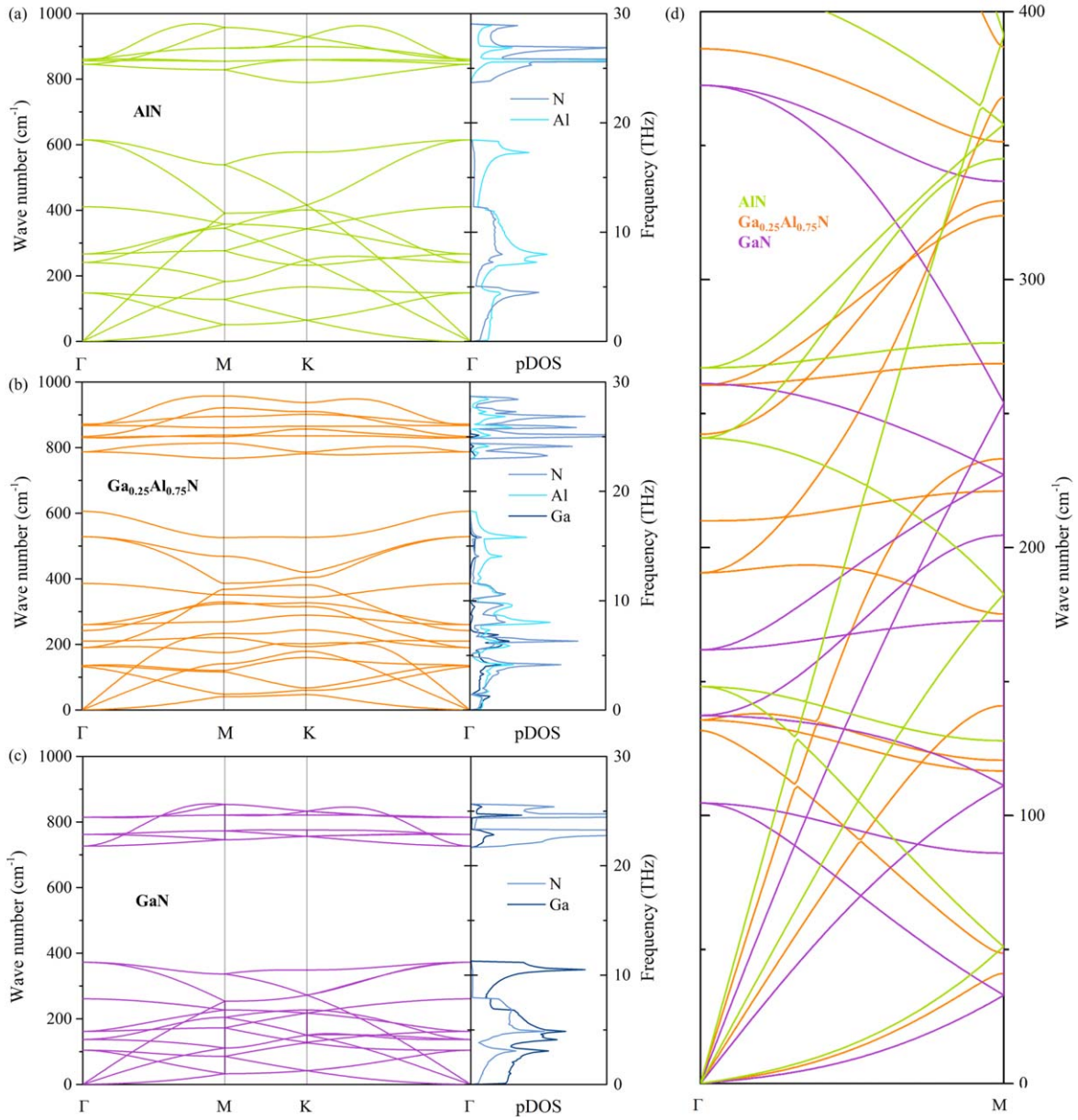

Figure 3. Phonon dispersions along the path passing through main high-symmetry *k*-points in irreducible Brillouin zone (IBZ) and the corresponding partial density of states (*p*DOS) for (a) AlN, (b) $Ga_{0.25}Al_{0.75}N$, and (c) GaN, respectively. (d) The three acoustic phonon branches labeled with FA, TA, and LA of each monolayer material along the Γ–M direction.

high in doped cases. In addition, the thermal conductivity as reported here are calculated with only three phonon scattering included while not including the possible four phonon scattering processes. Due to the much larger phonon scattering phase space compared to the three-phonon scatterings, four phonon scattering might be important for 2D materials with a large frequency gap [49], like the monolayer AlN, GaN and their alloy of $Ga_xAl_{1-x}N$ as studied in this work (figure 3). However, the gap in $Ga_{0.25}Al_{0.75}N$ is smaller than monolayer AlN and GaN, which means the possible four phonon scattering is relatively weaker in $Ga_{0.25}Al_{0.75}N$ than AlN and GaN. Thus, even with the four phonon scattering included, the thermal conductivity of $Ga_{0.25}Al_{0.75}N$ will still stand out visibly. Moreover, we would like to point out that the single-layer $Ga_xAl_{1-x}N$ alloy as studied in this work is in the free-standing form. In the case of supported by substrate in practical synthesis routes, the thermal transport properties of single-layer $Ga_xAl_{1-x}N$ alloy would change a lot due to effect of the substrate, which would be different for different substrates. For instance, the thermal conductivity of silicene has been either enhanced or suppressed by changing the surface crystal plane of the substrate [50]. The change of the thermal conductivity of single-layer $Ga_xAl_{1-x}N$ alloy would be critical and also depends on the specific substrate. Further studies are anticipated to address these questions for the effect of substrates, which are very interesting and deserve lots of endeavors.

To study the exceptionally high thermal conductivity of $Ga_{0.25}Al_{0.75}N$, the contribution from each phonon branch is extracted (figures 2(b)–(d)). Similar to the typical case of

graphene, the FA phonon branch predominantly contributes to the thermal conductivity for all the three systems as studied in this work. The reason might lie in the symmetry-based selection rule of phonon–phonon scattering in such planar structures [51]. Note that the optical phonon branches also contribute considerably to the thermal conductivity at 300 K for monolayer $Ga_{0.25}Al_{0.75}N$ as compared to GaN and AlN, And the percentage contribution keeps increasing as the temperature increase. The reason may lie in that, along with the increasing temperature, more high-frequency phonon modes are thermally excited, and simultaneously the phonon–phonon scattering becomes stronger for the low-frequency acoustic phonon modes.

The phonon dispersion curves along the Γ–M–K–Γ path and the corresponding partial density of states (*p*DOS) are shown in figure 3. For the purpose of comparison, the supercells of $2 \times 2 \times 1$ (8 atoms, being the same as $Ga_{0.25}Al_{0.75}N$, $Ga_{0.50}Al_{0.50}N$, $Ga_{0.75}Al_{0.25}N$) are used as the unit cell of AlN and GaN. Also plotted are the results of AlN and GaN with primitive cell (2 atoms) in Supplemental figure 3. It is obviously shown that the band gap of monolayer $Ga_{0.25}Al_{0.75}N$ is narrow compared to that of the original monolayer GaN, and is even a little bit smaller than that of AlN. Generally, the underlying mechanism of the narrowing band gap can be attributed to the smaller mass difference. The atomic masses are 69.72, 26.98, and 14.01 for Ga, Al, and N, respectively. As for the $Ga_{0.25}Al_{0.75}N$ with the existence of Al atoms, the largest mass difference is between Ga and Al atoms, being 42.74, which is smaller than that in GaN (55.71) while larger than that in AlN (12.97) [52]. In addition to the mass difference, as the phonon-spectra linkers, the Al atoms also bridge the vibrational mismatch between Ga and N atoms [53], which can enhance the thermal transport in $Ga_xAl_{1-x}N$ alloys to some extent. Note that there exists an obviously isolated optional phonon branch around 18 THz in the phonon dispersion of monolayer $Ga_{0.25}Al_{0.75}N$ as shown in figure 3(b), which cannot be probed in the monolayer $Ga_{0.5}Al_{0.5}N$ and $Ga_{0.75}Al_{0.25}N$ (supplemental figures 4(a) and (b)). The isolated optical phonon branch largely narrows the bandgap of $Ga_{0.25}Al_{0.75}N$ and leads to its narrowest bandgap compared to GaN and AlN, despite that the mass difference in $Ga_{0.25}Al_{0.75}N$ is not the smallest. As confirmed in the *p*DOS, the isolated optical phonon branch is contributed by the existing Al atoms in $Ga_{0.25}Al_{0.75}N$.

The percentage contribution of the isolated optical phonon branch around 18 THz in the $Ga_{0.25}Al_{0.75}N$ alloys is 0.27% at 300 K. Despite its low percentage contribution to the thermal transport, the isolated optical phonon branch plays a key role in affecting the phonon–phonon scattering processes by affecting the scattering phase space. On one hand, the isolated branch strengthens the coupling between the low-frequency phonon branches below the gap and the high-frequency optical phonon branches above the gap, leading to the enhanced phonon–phonon scattering. On the other hand, the branch is isolated from the low-frequency phonon branches below the gap and thus will weaken the coupling among them, leading to the weakened phonon–phonon scattering. Therefore, the thermal conductivity of $Ga_{0.25}Al_{0.75}N$ is governed by such a competitive mechanism driven by the isolated optical phonon branch.

The phonon dispersions of the monolayer GaN, $Ga_{0.25}Al_{0.75}N$, and AlN along the Γ−X direction are further demonstrated in figure 3(d). The FA phonon branch reveals a flexural characteristic, which is the unique feature for 2D materials, such as graphene [54], silicone [55], monolayer BN [56], etc. Note that the order of the phonon branch slope either for the TA or LA phonon modes [57] is proportional to the corresponding group velocity, which keeps in good agreement with the thermal conductivity of the three materials.

To further study the exceptionally high thermal conductivity of monolayer $Ga_{0.25}Al_{0.75}N$, comparative mode level analysis among monolayer GaN, $Ga_{0.25}Al_{0.75}N$, and AlN as revealed in figure 4 are conducted to explore the essential difference. The color map visually illustrates the modal contributions to the thermal conductivity. The overall phonon group velocities exhibited in figures 4(a)–(c) and also supplemental figure 5(a) are consistent with the slopes of phonon dispersions as shown in figure 3(d). Specifically, the group velocity of monolayer GaN and $Ga_{0.25}Al_{0.75}N$ is significantly smaller than that of AlN, which gives a straightforward explanation for the largest thermal conductivity of monolayer AlN compared to the other two materials based on the definition of thermal conductivity.

In addition, the modal phonon scattering rate is plotted in figures 4(d)–(f) and also Supplemental figure 5(b). It is found that the phonon scattering rate of monolayer GaN is dramatically larger than $Ga_{0.25}Al_{0.75}N$ and AlN. The reason may partially lie in the large difference in the atomic masses and radius of Ga and N atoms. As analyzed in previous studies, the large difference in the atomic radius and mass of Ga and N makes the planar not as smooth as graphene and then partially breaks the symmetry-based selection rule of phonon–phonon scattering [51], which has a negative effect on the thermal transport. The existence of Al atoms in $Ga_{0.25}Al_{0.75}N$ decreases the difference in atomic radius and mass of $Ga_{0.25}Al_{0.75}N$ compared to GaN. Consequently, the scattering rate of monolayer $Ga_{0.25}Al_{0.75}N$ can stay at the same level asAlN, being much lower than GaN.

It is well known that the scattering rate is governed by both the phonon anharmonicity and phonon scattering phase space, which determine the scattering strength and scattering possibility, respectively. The Grüneisen parameter which quantifies the parent is calculated for the three systems as shown in figures 4(g)–(i) and also supplemental figure 5(c) for a more in-depth study. It is obviously shown that the phonon scattering intensity of monolayer $Ga_{0.25}Al_{0.75}N$ and GaN keep the same level with each other but stronger than AlN, especially for the low-frequency phonon modes. In addition, the phonon–phonon scattering phase spaces (figures 4(j)–(l)) are also calculated for further analysis of the phonon scattering processes. Here, the phonon scattering process is decomposed into absorption and emission processes, respectively (see supplemental materials for more detailed information). It is valuable to note that the phase space of monolayer GaN even reaches up to 10^{-7} (containing both the

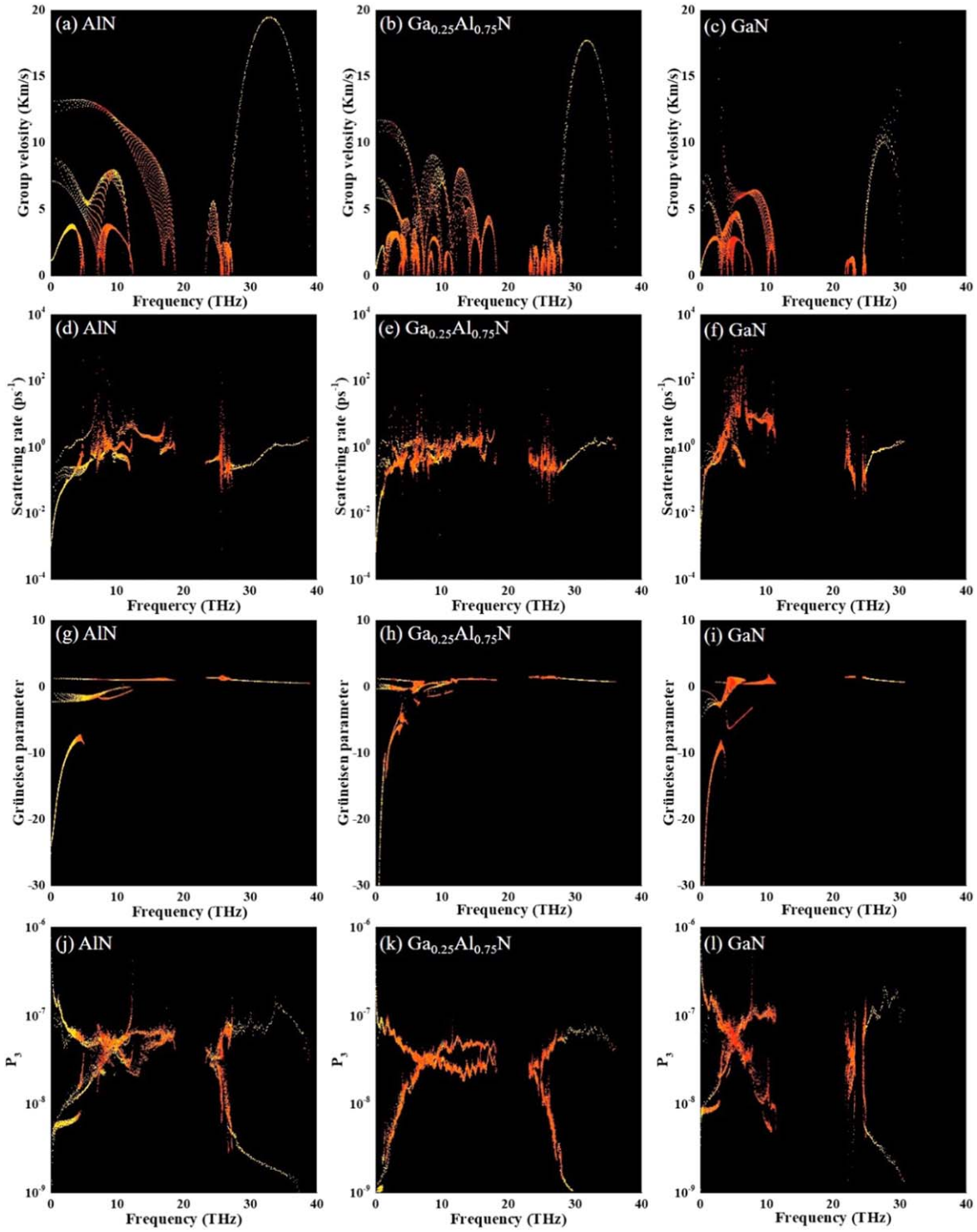

Figure 4. Modal analysis of thermal transport. (a)–(c) Phonon group velocity, (d)–(f) phonon scattering rate, (g)–(i) Grüneisen parameter and (j)–(l) volume in phase space as a function of frequency for monolayer AlN, $Ga_{0.25}Al_{0.75}N$, and GaN, respectively. The color maps are coded by the modal contributions to thermal conductivity, which ranges from red (low) to yellow (high).

absorption and emission processes) at low frequency. Together with the large phonon anharmonicity as revealed in figure 4(i), the largest phase space of GaN dominates the phonon scattering process and results in the larger scattering rate than $Ga_{0.25}Al_{0.75}N$ and AlN. Beyond that, the phase space of the AlN is slightly larger than $Ga_{0.25}Al_{0.75}N$ in either the absorption or emission processes. Combing with the relatively smaller Grüneisen parameter of AlN, the phonon scattering rate of AlN stays at the same level as that of $Ga_{0.25}Al_{0.75}N$.

Note that the phase space is calculated based on the conservation of both phonon energy and momentum [58, 59], which is governed by the phonon dispersions (see supplemental materials for more detailed information). As analyzed

above based on figure 3(b), the isolated optical phonon branch around 18 THz in the phonon dispersion of $Ga_{0.25}Al_{0.75}N$ will lead to the competitive effect on the scattering phase space. The relatively small phase space of $Ga_{0.25}Al_{0.75}N$ as revealed in figure 4(e) evidently shows that the effect of the isolated optical phonon branch on weakening coupling of the low-frequency phonon branches below the gap is stronger than the effect on strengthening coupling between the low-frequency phonon branches below the gap and the high-frequency optical phonon branches above the gap. In addition, such results also reveal the key role of the isolated optical phonon branch in resulting in the exceptionally high thermal conductivity of $Ga_{0.25}Al_{0.75}N$ by affecting the phonon–phonon scattering processes. It is clear to see that the thermal conductivity of the AlN, $Ga_{0.25}Al_{0.75}N$, and GaN keep in good agreement with above analysis.

In short, the smaller thermal conductivity of $Ga_{0.25}Al_{0.75}N$ than AlN is due to the smaller group velocity. At the same time, the same level scattering rate of $Ga_{0.25}Al_{0.75}N$ and AlN is due to the counterbalance of Grüneisen parameter and phase space. On the other hand, the larger thermal conductivity of $Ga_{0.25}Al_{0.75}N$ than GaN is due to both the larger group velocity and smaller scattering rate, which can be understood from the smaller phase space of $Ga_{0.25}Al_{0.75}N$ than GaN driven by the isolated optical phonon branch.

To further understand the underlying mechanism for the exceptionally high thermal conductivity of $Ga_{0.25}Al_{0.75}N$ achieved by 'alloying' GaN and AlN, insight is gained into the behavior of electrons in the three materials. The comparative analysis is performed based on the orbital projected electronic density of states (*p*DOS) and the electron localization function (ELF). As shown in figure 5(a), there exists sp^2 hybridization in monolayer AlN and the valance band maximum is mainly contributed from the N-*p*, Al-*p,* and Al-*s* orbitals, which form the strong covalent Al–N bonding (figures 5(d), (g)). As for the case of GaN (figures 5(c), (f), (j)), the strong covalent Ga–N bond is also formed based on the sp^2 hybridization, which is mediated by the Ga-*d* orbital as reported in our previous work [53]. Because of the large difference in the electronegativity between Ga and N atoms, the Ga–N bond is strongly polarized as revealed by the ELF (figures 5(f), (j)). When forming the $Ga_{0.25}Al_{0.75}N$ by alloying GaN and AlN, the orbital hybridization becomes slightly different. Compared to that in GaN and AlN, the contribution of N-*p* orbital to the bonding sp^2 hybridization decreased apparently in $Ga_{0.25}Al_{0.75}N$, while the contribution from Ga-*p* and Ga-*d* shows a clear trend of enhancement. As a result, the polarization of Ga–N bond in $Ga_{0.25}Al_{0.75}N$ is weakened compared to that in GaN. Such a phenomenon is evidently shown in the ELF (figures 5(e), (h), (i)). As analyzed in previous study [54], the strong polarization of bond could lead to low thermal conductivity by strengthening the phonon–phonon scattering. Thus, the weakened polarization of bonding in $Ga_{0.25}Al_{0.75}N$ compared to GaN might be partially responsible for its larger thermal conductivity than GaN. At the same time, the bond length of Ga–N bond (1.876 Å) in $Ga_{0.25}Al_{0.75}N$ is a little bit shorter than that in GaN (1.879 Å). Thus, the Ga–N bond in $Ga_{0.25}Al_{0.75}N$ is stronger, which explains the larger group velocity in $Ga_{0.25}Al_{0.75}N$ than GaN (figures 4(b), (c)).

Based on the above analysis, we could expect that, as for other group-III nitrides or arsenides monolayers, the thermal conductivity of alloys like the monolayer $Ga_xAl_{1-x}N$ may be found when mismatched atomic radius, masses. and electronegativity happen in the corresponding proportion of the alloy. However, it must be pointed out that the above proposal needs to be further verified by reasonable calculations. The influence factors can also be different depending on the different atoms when forming alloy, which is an interesting issue that can be explored in future studies. Here, we only focus on the widely applied AlN, GaN. and their alloys to probe and broaden its practical application values. In fact, to extend the universality of high thermal conductivity of alloys, the monolayer BN, AlN, and their alloys $B_xAl_{(1-x)}N$ ($x = 0.25$, 0.5, 0.75) have been further employed to verify the regularity at the same time. Unfortunately, the considerable imaginary frequencies shown in the phonon spectra of all the three configurations of the $B_xAl_{(1-x)}N$ alloy reveal the unstable structures and prevent the exploration for the next step (supplemental figure 6).

Conclusions

In summary, we comparatively investigated the thermal transport in the monolayer GaN, AlN. and their alloy $Ga_{0.25}Al_{0.75}N$ by solving the first-principles based BTE. The thermal conductivity of monolayer $Ga_{0.25}Al_{0.75}N$ (29.57 Wm^{-1} K^{-1}) is found to be exceptionally high and between parent materials of AlN (74.42 Wm^{-1} K^{-1}) and GaN (14.92 Wm^{-1} K^{-1}), which breaks the common rule of alloying lowering thermal conductivity. The first reason for this anomalous phenomenon is analyzed to be the reduced difference in atomic radius and masses of the $Ga_{0.25}Al_{0.75}N$ alloy, which has a positive effect on the symmetry-based selection rule of phonon–phonon scattering along with the planar structure. Besides, the isolated optical phonon branch around 18 THz in the phonon dispersion of $Ga_{0.25}Al_{0.75}N$ due to the existing Al atoms is found to play a key role, which reduces phonon–phonon scattering by weakening the coupling among the low-frequency phonon branches below the gap. Deep analysis from the *p*DOS and ELF further provides insight that the alloying process weakens the polarization of bonding in $Ga_{0.25}Al_{0.75}N$ and leads to the increased thermal conductivity. The exceptionally high thermal conductivity of the $Ga_{0.25}Al_{0.75}N$ alloy and the underlying mechanism as revealed in this study would bring valuable insight for the future research of materials especially for the group-III nitrides or arsenides monolayers with applications in high-performance thermal management.

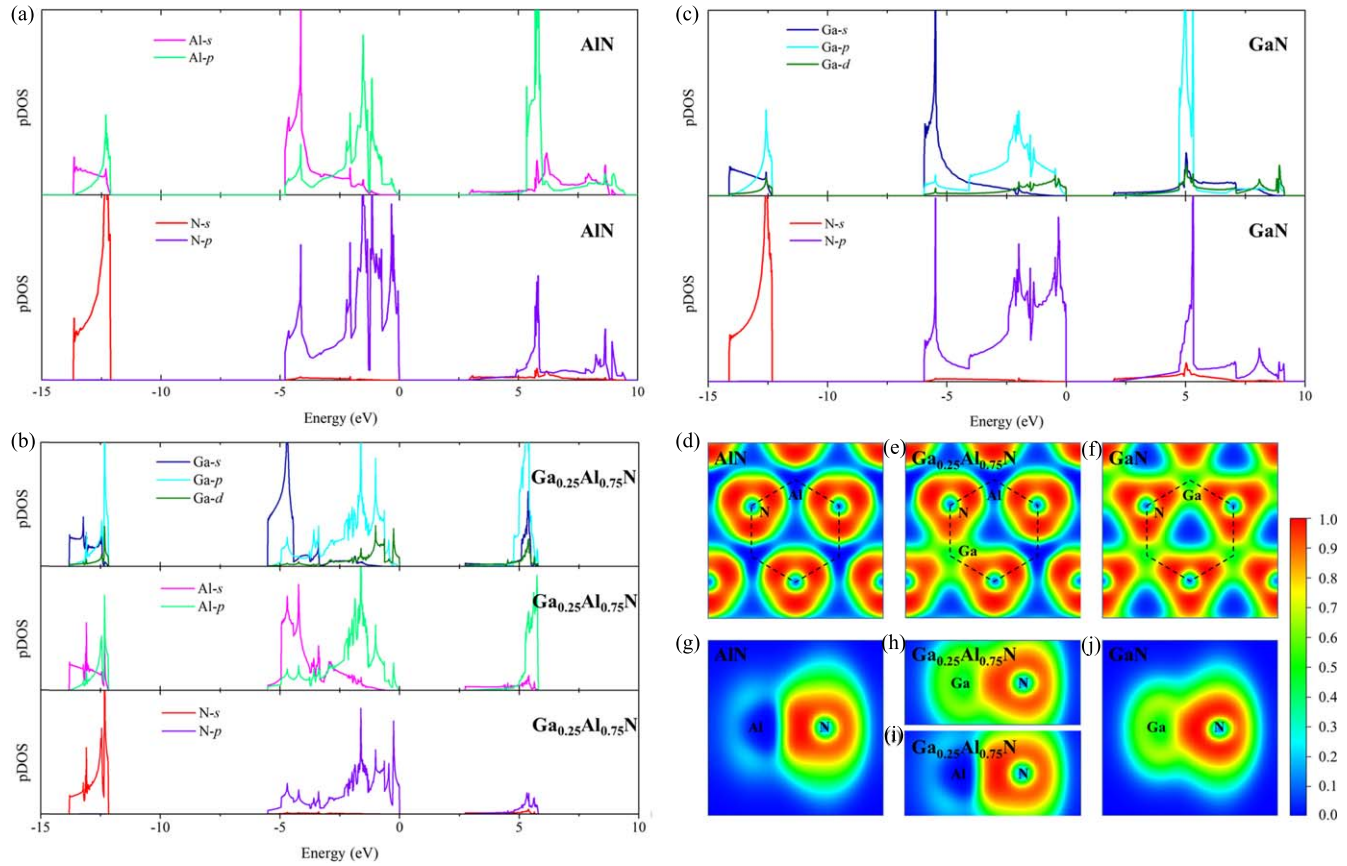

Figure 5. The orbital projected electronic density of states (*p*DOS) of (a) AlN, (b) $Ga_{0.25}Al_{0.75}N$ and (c) GaN. (d)–(f) Top and (g)–(j) side views of the electron localization function (ELF).

Acknowledgments

This work was supported by the National Key R&D Program of China (No. 2017YFB0406000) and the National Natural Science Foundation of China (Nos. 51906097, 52006057, 11904324, 51972162, 11847158), the China Postdoctoral Science Foundation (2018M642776), and the Fundamental Research Funds for the Central Universities (Grant No. 531118010471). Research reported in this publication was also supported in part by the NSF (award number 1905775) and SC EPSCoR/IDeA Program under NSF OIA-1655740 via SC EPSCoR/IDeA 20-SA05. The numerical calculations in this paper have been done on the supercomputing system of the National Supercomputing Center in Changsha.

Data availability

The datasets generated during and/or analyzed during the current study are available from the corresponding author on reasonable request.

Author contributions

H M Wang and D H Wei were responsible for the investigation, methodology, data curation, and initial draft of the paper. The calculations were carried out supervised by G Z Qin. Z Z Qin and J F Duan participated in the discussion and provided insightful suggestions. The whole project was supervised by G Z Qin, Y G Yao and M Hu. All authors contributed to the manuscript writing. H M Wang and D H Wei contribute equally to this work.

Competing interests

The authors declare no competing interests.

ORCID iDs

Huimin Wang https://orcid.org/0000-0003-3436-9423
Guangzhao Qin https://orcid.org/0000-0001-6770-1096
Ming Hu https://orcid.org/0000-0002-8209-0139

References

[1] Chhowalla M, Jena D and Zhang H 2016 Two-dimensional semiconductors for transistors *Nat. Rev. Mater.* **1** 16052
[2] Le Lay G 2015 Silicene transistors *Nat. Nanotechnol.* **10** 202–3
[3] Yang X *et al* 2018 Efficient green light-emitting diodes based on quasi-two-dimensional composition and phase

engineered perovskite with surface passivation *Nat. Commun.* **9** 570
[4] Xia F, Wang H, Xiao D, Dubey M and Ramasubramaniam A 2014 Two-dimensional material nanophotonics *Nat. Photon.* **8** 899–907
[5] Khan A H *et al* 2017 Two-dimensional (2D) nanomaterials towards electrochemical nanoarchitectonics in energy-related applications *BCS J.* **90** 627–48
[6] Schwierz F 2010 Graphene transistors *Nat. Nanotechnol.* **5** 487–96
[7] Li D and Kaner R B 2008 Graphene-based materials *Science* **320** 1170
[8] Madhushankar B N *et al* 2017 Electronic properties of germanane field-effect transistors *2D Mater.* **4** 021009
[9] Koski K J and Cui Y 2013 The new skinny in two-dimensional nanomaterials *ACS Nano* **7** 3739–43
[10] Cai Y, Chuu C-P, Wei C M and Chou M Y 2013 Stability and electronic properties of two-dimensional silicene and germanene on graphene *Phys. Rev.* B **88** 245408
[11] Yan J-A, Stein R, Schaefer D M, Wang X-Q and Chou M Y 2013 Electron–phonon coupling in two-dimensional silicene and germanene *Phys. Rev.* B **88** 121403
[12] Li X and Zhu H 2015 Two-dimensional MoS_2: properties, preparation, and applications *J. Materiomics* **1** 33–44
[13] Scalise E, Houssa M, Pourtois G, Afanas'ev V and Stesmans A 2012 Strain-induced semiconductor to metal transition in the two-dimensional honeycomb structure of MoS_2 *Nano Res.* **5** 43–8
[14] Lehtinen O *et al* 2015 Atomic scale microstructure and properties of se-deficient two-dimensional $MoSe_2$ *ACS Nano* **9** 3274–83
[15] Golberg D *et al* 2010 Boron nitride nanotubes and nanosheets *ACS Nano* **4** 2979–93
[16] Prete M S, Mosca Conte A, Gori P, Bechstedt F and Pulci O 2017 Tunable electronic properties of two-dimensional nitrides for light harvesting heterostructures *Appl. Phys. Lett.* **110** 012103
[17] Taniyasu Y, Kasu M and Makimoto T 2006 An aluminium nitride light-emitting diode with a wavelength of 210 nanometres *Nature* **441** 325–8
[18] Kim D-H *et al* 2005 Enhanced light extraction from GaN-based light-emitting diodes with holographically generated two-dimensional photonic crystal patterns *Appl. Phys. Lett.* **87** 203508
[19] Nakamura S, Mukai T and Senoh M 1994 Candela-class high-brightness InGaN/AlGaN double-heterostructure blue-light-emitting diodes *Appl. Phys. Lett.* **64** 1687–9
[20] Denbaars S P 1997 Gallium-nitride-based materials for blue to ultraviolet optoelectronics devices *Proc. IEEE* **85** 1740–9
[21] Zhao S *et al* 2016 Molecular beam epitaxy growth of Al-rich AlGaN nanowires for deep ultraviolet optoelectronics *APL Mater.* **4** 086115
[22] Xia C, Peng Y, Wei S and Jia Y 2013 The feasibility of tunable p-type Mg doping in a GaN monolayer nanosheet *Acta Mater.* **61** 7720–5
[23] Zhao Q *et al* 2016 Tuning magnetism of monolayer GaN by vacancy and nonmagnetic chemical doping *J. Phys. Chem. Solids* **91** 1–6
[24] Gao N *et al* 2019 Integral monolayer-scale featured digital-alloyed AlN/GaN superlattices using hierarchical growth units *Cryst. Growth Des.* **19** 1720–7
[25] Gillet J-N, Chalopin Y and Volz S 2009 Atomic-scale three-dimensional phononic crystals with a very low thermal conductivity to design crystalline thermoelectric devices *J. Heat Transfer* **131** 043206
[26] Li G *et al* 2015 Efficient light-emitting diodes based on nanocrystalline perovskite in a dielectric polymer matrix *Nano Lett.* **15** 2640–4
[27] Tadjer M J *et al* 2012 Reduced self-heating in AlGaN/GaN HEMTs using nanocrystalline diamond heat-spreading films *IEEE Electron Device Lett.* **33** 23–5
[28] Asif Khan M, Bhattarai A, Kuznia J N and Olson D T 1993 High electron mobility transistor based on a GaN–$Al_xGa_{1-x}N$ heterojunction *Appl. Phys. Lett.* **63** 1214–5
[29] Fu T *et al* 2016 Enhanced thermoelectric performance of PbTe bulk materials with figure of merit ZT >2 by multi-functional alloying *J. Materiomics* **2** 141–9
[30] Gell M A *et al* 1987 Effects of alloying and hydrostatic pressure on electronic and optical properties of GaAs–$Al_xGa_{1-x}As$ superlattices and multiple-quantum-well structures *Phys. Rev.* B **35** 1196–222
[31] Komsa H-P and Krasheninnikov A V 2012 Two-dimensional transition metal dichalcogenide alloys: stability and electronic properties *J. Phys. Chem. Lett.* **3** 3652–6
[32] Li W, Lindsay L, Broido D A, Stewart D A and Mingo N 2012 Thermal conductivity of bulk and nanowire $Mg_2Si_xSn_{1-x}$ alloys from first principles *Phys. Rev.* B **86** 174307
[33] Gu X and Zhao C Y 2019 Thermal conductivity of single-layer $MoS_{2(1-x)}Se_{2x}$ alloys from molecular dynamics simulations with a machine-learning-based interatomic potential *Comput. Mater. Sci.* **165** 74–81
[34] Ma J, Li W and Luo X 2016 Intrinsic thermal conductivities and size effect of alloys of wurtzite AlN, GaN, and InN from first-principles *J. Appl. Phys.* **119** 125702
[35] Kresse G and Furthmüller J 1996 Efficient iterative schemes for *ab initio* total-energy calculations using a plane-wave basis set *Phys. Rev.* B **54** 11169–86
[36] Perdew J P, Burke K and Ernzerhof M 1996 Generalized gradient approximation made simple *Phys. Rev. Lett.* **77** 3865–8
[37] Qin G, Qin Z, Wang H and Hu M 2017 Anomalously temperature-dependent thermal conductivity of monolayer GaN with large deviations from the traditional 1/T law *Phys. Rev.* B **95** 195416
[38] Monkhorst H J and Pack J D 1976 Special points for Brillouin-zone integrations *Phys. Rev.* B **13** 5188–92
[39] Lindsay L, Broido D A and Reinecke T L 2012 Thermal conductivity and large isotope effect in GaN from first principles *Phys. Rev. Lett.* **109** 095901
[40] Abeles B 1963 Lattice thermal conductivity of disordered semiconductor alloys at high temperatures *Phys. Rev.* **131** 1906–11
[41] Larkin J M and McGaughey A J H 2013 Predicting alloy vibrational mode properties using lattice dynamics calculations, molecular dynamics simulations, and the virtual crystal approximation *J. Appl. Phys.* **114** 023507
[42] Bao H, Chen J, Gu X and Cao B 2018 A review of simulation methods in micro/nanoscale heat conduction *ES Energy Environ* **1** 16–55
[43] Togo A, Oba F and Tanaka I 2008 First-principles calculations of the ferroelastic transition between rutile-type and$CaCl_2$-type SiO_2 at high pressures *Phys. Rev.* B **78** 134106
[44] Li W, Carrete J, Katcho A N and Mingo N 2014 ShengBTE: a solver of the Boltzmann transport equation for phonons *Comput. Phys. Commun.* **185** 1747–58
[45] Zhao L, Xu S, Wang M and Lin S 2016 Probing the thermodynamic stability and phonon transport in two-dimensional hexagonal aluminum nitride monolayer *J. Phys. Chem.* C **120** 27675–81
[46] Qin Z, Qin G, Zuo X, Xiong Z and Hu M 2017 Orbitally driven low thermal conductivity of monolayer gallium nitride (GaN) with planar honeycomb structure: a comparative study *Nanoscale* **9** 4295–309
[47] Cepellotti A *et al* 2015 Phonon hydrodynamics in two-dimensional materials *Nat. Commun.* **6** 6400

[48] Liao B *et al* 2015 Significant reduction of lattice thermal conductivity by the electron–phonon interaction in silicon with high carrier concentrations: a first-principles study *Phys. Rev. Lett.* **114** 115901
[49] Feng T, Lindsay L and Ruan X 2017 Four-phonon scattering significantly reduces intrinsic thermal conductivity of solids *Phys. Rev.* B **96** 161201
[50] Zhang X and Bao H 2015 Bilateral substrate effect on the thermal conductivity of two-dimensional silicon *Nanoscale* **7** 6014–22
[51] Lindsay L, Broido D A and Mingo N 2010 Flexural phonons and thermal transport in graphene *Phys. Rev.* B **82** 115427
[52] Gu X and Yang R 2014 Phonon transport in single-layer transition metal dichalcogenides: a first-principles study *Appl. Phys. Lett.* **105** 131903
[53] Chen X and Chen K 2020 Thermal transport of carbon nanomaterials *J. Phys.: Condens. Matter* **32** 153002
[54] Castro Neto A H, Guinea F, Peres N M R, Novoselov K S and Geim A K 2009 The electronic properties of graphene *Rev. Mod. Phys.* **81** 109–62
[55] Zhang X *et al* 2014 Thermal conductivity of silicene calculated using an optimized Stillinger–Weber potential *Phys. Rev.* B **89** 054310
[56] Tabarraei A 2015 Thermal conductivity of monolayer hexagonal boron nitride nanoribbons *Comput. Mater. Sci.* **108** 66–71
[57] Zhu Z and Tománek D 2014 Semiconducting layered blue phosphorus: a computational study *Phys. Rev. Lett.* **112** 176802
[58] Ward A and Broido D A 2010 Intrinsic phonon relaxation times from first-principles studies of the thermal conductivities of Si and Ge *Phys. Rev.* B **81** 085205
[59] Ward A, Broido D A, Stewart D A and Deinzer G 2009 *Ab initio* theory of the lattice thermal conductivity in diamond *Phys. Rev.* B **80** 125203